INSTITUTE OF PHYSICS PUBLISHING NANOTECHNOLOGY
Nanotechnology **18** (2007) 044028 (5pp) doi:10.1088/0957-4484/18/4/044028

Ultrafast photoinduced carrier dynamics in GaNAs probed using femtosecond time-resolved scanning tunnelling microscopy

Yasuhiko Terada, Masahiro Aoyama, Hiroyuki Kondo, Atsushi Taninaka, Osamu Takeuchi and Hidemi Shigekawa[1]

Institute of Applied Physics, 21st COE, CREST-JST, University of Tsukuba, Tsukuba 307-8573, Japan

Received 16 August 2006, in final form 5 December 2006
Published 21 December 2006
Online at stacks.iop.org/Nano/18/044028

Abstract
The combination of scanning tunnelling microscopy (STM) with optical excitation using ultrashort laser pulses enables us, in principle, to simultaneously obtain ultimate spatial and temporal resolutions. We have developed the shaken-pulse-pair-excited STM (SPPX-STM) and succeeded in detecting a weak time-resolved tunnelling current signal from a low-temperature-grown GaNAs sample. To clarify the underlying physics in SPPX-STM measurements, we performed optical pump–probe reflectivity measurements with a wavelength-changeable ultrashort-pulse laser. By comparing the results obtained from the two methods with an analysis based on the nonlinear relationship between the photocarrier density and tunnelling current, we obtained a comprehensive explanation that the photocarrier dynamics is reflected in the SPPX-STM signal through the surface photovoltage effect.

(Some figures in this article are in colour only in the electronic version)

1. Introduction

At present, 'smaller' and 'faster' are the main concepts in nanoscale science and technology. Indeed, important and interesting phenomena in various systems, such as those in functional materials, electronic devices, signal transfer in biosystems and chemical reactions, have been observed on scales from several tens of a nanometre to subnanometres in space and from several tens of a picosecond to subpicoseconds in time. However, it is extremely difficult to simultaneously obtain spatial and temporal resolutions on these scales. Therefore, to determine the possibility of realizing such resolutions, it is necessary to develop a new method, that is, laser-combined scanning tunnelling microscopy (STM) which will enable us to observe the dynamics of electronic structures at the ultimate spatial and temporal resolutions.

Among the numerous approaches previously reported concerning time-resolved STM [1–7], the shaken-pulse-pair-excited STM (SPPX-STM) has turned out to be promising for detecting weak time-resolved tunnelling currents at a high spatial resolution [8–13]. In SPPX-STM measurements, the sample surface under the STM tip is illuminated by a sequence of ultrashort laser pulse pairs and the variation in the tunnelling current is measured as a function of the delay time between the two pulses in each pulse pair. When the transient current has a nonlinear relationship with the laser intensity, the average tunnelling current depends on the delay time. Thus, although we cannot detect an ultrafast transient current using STM because of the limited bandwidth of the current–voltage converter, ∼100 kHz, we can observe the temporal change of the photoinduced phenomena through the change in the average tunnelling current. The observed time-resolved current involves various complicated physical processes induced in a sample. Furthermore, SPPX-STM essentially requires a

[1] http://dora.ims.tsukuba.ac.jp

Table 1. Parameters derived from SPPX-STM and OPPR measurements.

	SPPX-STM		OPPR		
			B_i	τ_i^{OPPR} (ps)	τ_i^{OPPR} (ps)
	A_i (pA)	τ_i^{STM} (ps)	(1 mW[a])		(Average[b])
$i=1$	48.6 ± 4.9	118 ± 7	$(-2.02 \pm 0.02) \times 10^{-4}$	7.59 ± 0.04	5.3 ± 1.6
$i=2$	-21.4 ± 1.3	550 ± 300	$(9.57 \pm 0.01) \times 10^{-5}$	406 ± 2	400 ± 40

[a] Pump intensity.
[b] Average of the values for all pump intensities in figure 4.

highly nonlinear relationship between the tunnelling current and laser intensity. Accordingly, the interpretation of SPPX-STM signals is not straightforward [12]. The extraction of the ultrafast physical properties from observed time-resolved signals requires a detailed understanding of the physical processes that contribute to tunnelling. In this study, we examined how the ultrafast photocarrier decay process is reflected in the SPPX-STM spectra.

2. Experimental details

Low-temperature-grown GaN_xAs_{1-x} ($x = 0.36\%$, grown at 720 K) was used as a sample. The energy bandgap E_g was estimated to be 1.34 eV (923 nm) from the photoluminescence spectra measured at 300 K. Each of the mode-locked Ti:sapphire laser pulses (pulse width <130 fs, central wavelength: 800 nm, repetition rate: 80 MHz for SPPX-STM and 90 MHz for optical pump–probe reflectivity (OPPR) measurements) was divided into two pulses to form a train of pulse pairs (pump and probe pulses) with a delay time. We controlled the delay time between pump and probe pulses by changing the optical length of the delay system.

For SPPX-STM measurements [8, 10], the sample surface under the STM tip was illuminated at the average intensity of 0.8 mW and the spot diameter of ~10 μm. Thus the average tunnelling current was measured as a function of the delay time τ. For simplicity, the pump and probe powers were adjusted to be the same to avoid the asymmetry in the SPPX-STM signal against $\tau = 0$ [12]. The STM set-point tunnelling current and sample bias voltage were 200 pA and 406 mV, respectively. The delay time was modulated at 31 Hz with an amplitude of 6 ps, and the corresponding change in the tunnelling current, $\mathrm{d}(\Delta I)/\mathrm{d}\tau$ with respect to the delay time, was measured by the lock-in detection technique. The time constant of the lock-in amplifier was 100 ms and the decay slope was −24 dB/oct. The time-resolved tunnelling current ΔI was obtained by integrating the raw signal.

For OPPR measurements, the average power of the probe beam was set to be 1/10 that of the pump beam, both of which were focused to a 10 μm diameter spot on the sample surface. The pump beam was chopped at 80 Hz and the corresponding change in probe reflectivity was measured as a function of the delay time using a silicon photodiode and lock-in amplifier. The maximum density of photoexcited carriers was estimated to be 2.8×10^{17} cm^{-3} from the pump power density of 950 mW cm^{-2} and the absorption coefficient of 3.4×10^4 cm^{-1}.

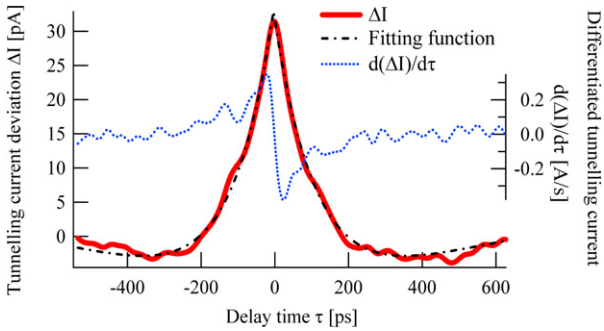

Figure 1. SPPX-STM signal with the fitting function. Adjusted fitting parameters are summarized in table 1.

3. Results and discussion

3.1. SPPX-STM signal

3.1.1. SPPX-STM spectra. First, let us examine the photoinduced dynamics observed using SPPX-STM. Figure 1 is the raw data of the differentiated tunnelling current $\mathrm{d}(\Delta I)/\mathrm{d}\tau$ (blue/dotted) and the numerically integrated time-resolved tunnelling current ΔI (red/solid). Since the integral constant cannot be determined in the experiment, the left end of the ΔI curve was taken to be zero. Figure 1 also shows the fitting function (black/dashed–dotted) consisting of the sum of two exponential functions and a constant, $\Sigma_i A_i \exp(-\tau/\tau_i^{\mathrm{STM}}) + \mathrm{const}$ ($i = 1, 2$), that gives the best fit to the ΔI curve. Parameters adjusted to fit are summarized in table 1. Since the ΔI curve is sufficiently symmetric against $\tau = 0$, we hereafter consider only the positive region $\tau > 0$.

The ΔI curve consists of two decay components that reflect the ultrafast phenomena induced by laser illumination. The faster component ($\tau_1^{\mathrm{STM}} = 118$ ps) has a positive amplitude ($A_1 > 0$), while the slower one ($\tau_2^{\mathrm{STM}} = 550$ ps) has a negative amplitude ($A_2 < 0$). The characteristic of the faster component (Type-1) is similar to that observed previously [8–10], but the slower one (Type-2) was observed for the first time because the time constant τ_2^{STM}(550 ps) was much longer than the scan range limit of the delay time in the previous experimental setup. The characteristic properties of the two components were similar for both negative and positive sample bias voltages.

In the next section, we will consider how the photocarrier decay process is reflected in the delay time dependence of ΔI.

3.1.2. What can be observed in the SPPX-STM signal? As discussed in the previous paper [12], a nonlinear response of the transient tunnelling current to the laser intensity

is necessary to produce a delay-time-dependent average tunnelling current (ΔI curve). The nonlinear dependence of tunnelling current on laser intensity is classified into two steps: (i) nonlinearity between the physical parameters of the samples and laser intensity and (ii) nonlinearity between the tunnelling current and the physical parameters. Here, the physical parameters include photocarrier density, plasmon density, electron temperature, electric polarization, lattice vibration amplitude and any other optically induced parameters that influence the tunnelling current.

Among the possible processes, the excitation and relaxation of photocarriers are considered to dominantly affect the ΔI curve. We hereafter focus on the photocarrier dynamics. In the previous study, the relationship between the decay of carrier density in real time and the ΔI curve was treated with a simple model, which revealed that ΔI curves exhibit different behaviours for the two different types of nonlinearity: (i) divergent and (ii) saturation-prone [12].

The divergent and saturation-prone nonlinearities are expressed here as $I_t(t) \propto n(t)^k$ $(k > 1)$ and $I_t(t) \propto n(t)^k$ $(k < 1)$, respectively, where I_t is the transient tunnelling current and n is the photocarrier density. Under the assumption of exponential decay of carrier density, $n(t) \sim \exp(-t/\tau_{decay})$, the divergent and saturation-prone nonlinearities result in characteristics similar to those of the faster (Type-1) and slower (Type-2) components observed for the SPPX-STM signal in figure 1, respectively. For the divergent nonlinearity ΔI has its maximum at $\tau = 0$ and decreases with increasing τ, whereas for the saturation-prone nonlinearity ΔI is minimum at $\tau = 0$ and increases with τ.

The Type-2 process is related to surface photovoltage (SPV). Under the STM measurement conditions on a semiconductor sample, the STM configuration has a metal–insulator–semiconductor (MIS) structure in which the STM tip induces a band bending in the sample surface in the dark [14]. When the surface is photo-illuminated, the band is flattened because of the spatial redistribution of photoexcited carriers. The resulting change in surface potential is referred to as SPV, which can be measured by STM with a high spatial resolution [14–17]. The SPV modifies the effective bias voltage at the tunnel junction, hence the relationship between the photocarrier density and SPV has a strong nonlinearity. The nonlinearity between the photocarrier density and SPV is saturation-prone because the SPV readily saturates with an increasing laser intensity. Therefore, the decay process of the photocarriers appears in the ΔI curve with the Type-2 characteristic.

For the Type-1 component, the dynamics may be related, for example, to multi-excitation of carriers, hot-carrier temperature, emission and reabsorption of hot phonons, the plasmon effect, carrier diffusion and drift. However, it is still under consideration and the mechanism of the Type-1 decay is left open for future investigation.

In the next section, we will discuss the results obtained from OPPR analysis.

4. Results of OPPR analysis

4.1. Band structure of GaNAs sample

In direct bandgap semiconductors such as GaAs, the photoexcited carriers form a hot, thermalized energy distribution on the subpicosecond timescale and are then cooled via phonon emission on a timescale of a few picoseconds [18]. The carrier cooling or energy relaxation occurs through various phonon scattering mechanisms which transfer the excess energy to the lattice, and the main one is the scattering of longitudinal optical (LO) phonons (figure 2(a)). In addition to the carrier cooling, the carrier density decays on the same or longer timescale through various processes: diffusion, recombination or trapping in deep states or defects (figure 2(b)). Although both the carrier cooling and decay may involve various processes, in the simplest picture under the assumption of a parabolic energy band structure, all the effects related to the cooling and decay can be incorporated in the phenomenological carrier cooling and decay times, τ_{cool} and τ_{decay}, respectively. In this approach, the lifetime of photocarriers is identical to τ_{decay}.

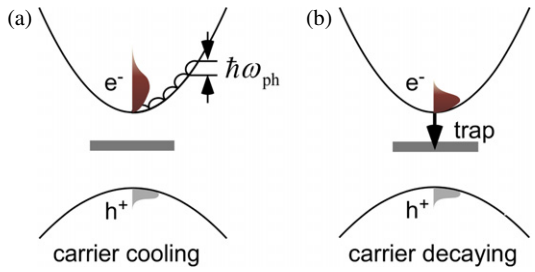

Figure 2. Schematic illustrations of the (a) cooling and (b) decay processes of the photoexcited carriers.

This simple approach, however, may not be valid for the GaNAs sample because the incorporation of nitrogen causes a change in the modification of the conduction band structure [19–21]: narrowing of the bandgap, increase in the effective electron mass and conduction-band splitting into E^- and E^+ bands. Although the former two effects can be incorporated in the parabolic approximation by adopting suitable values for the model parameters, the third one cannot be included; that is, the band splitting would produce different decay processes for photocarriers instead of a single decay time τ_{decay}.

Therefore the parabolic approximation is reasonable only when the photon energy is below the bandgap energy for the E^+ band, 1.74 eV [20], which is satisfied for the photon energy region (1.32–1.72 eV) of our experiment. In order to confirm this point, we performed OPPR measurements for various laser wavelengths (figure 3(a)). The band structure of the sample is illuminated by the cross section of OPPR traces (figure 3(b)), the 'photon energy dependence of OPPR spectra', where each spectrum shows a derivative-like feature at the photon energy corresponding to the red-shifted bandgap E_g (=1.34 eV). In addition to the bandgap of GaNAs, a small derivative feature is observed at 1.43 eV that might be attributed to the band structure of the GaAs substrate 1 μm below the GaNAs layer. No derivative-like feature other than these two features exists with excitation energies between 1.32 eV (940 nm) and 1.72 eV (720 nm) as expected. The decay process could therefore be analysed using a single decay time τ_{decay}, and the lifetime experimentally obtained was almost photon-energy-independent in this region, as will be described in the next section.

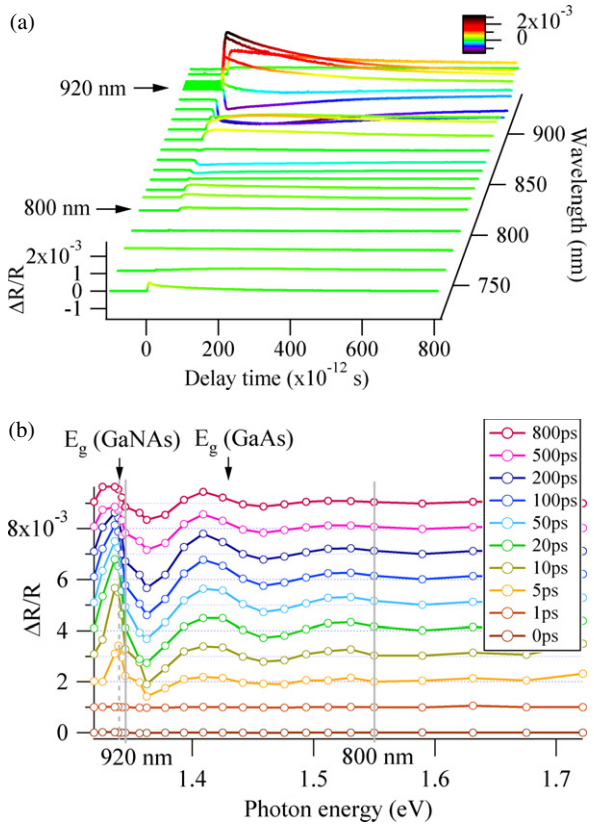

Figure 3. (a) OPPR spectra obtained for various laser wavelengths. (b) Cross sections of the OPPR traces in (a).

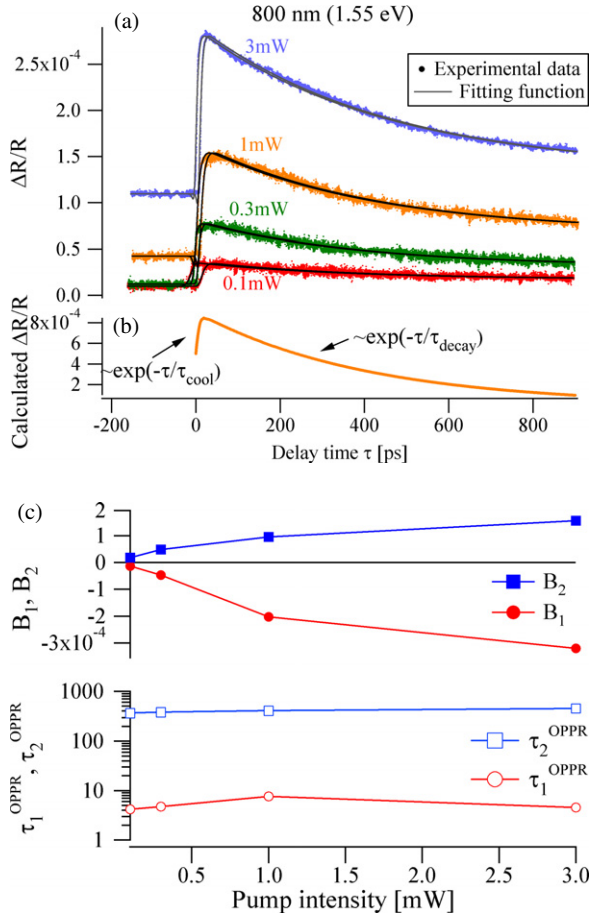

Figure 4. (a) OPPR traces obtained for various pump intensities. The excitation energy is 1.55 eV (800 nm) and the fitting functions (black lines) are shown together. (b) Results of the simulation with respect to the procedure reported in [20]. (c) Pump intensity dependence of the amplitudes and decay times of the two components of the OPPR signal.

4.2. Estimation of photocarrier lifetime by OPPR analysis

The lifetime of photocarriers was determined from the OPPR traces through fitting under the assumption of the sum of two exponential functions and a step function, $\Sigma_i B_i \exp(-\tau/\tau_i^{\mathrm{OPPR}}) + B_3$ $(i = 1, 2)$. The distortion due to the finite temporal width of laser pulses and the time constants of lock-in detection were taken into account.

Figure 4(a) shows the OPPR traces with the excitation energy of 1.55 eV (800 nm) and the best fits to the data. The fitting parameters are listed in table 1, together with the values obtained from SPPX-STM measurement. In order to identify the parameters with carrier cooling and decay times, we simulated the OPPR traces according to the procedure reported by Prabhu *et al* [23]. Our calculation took into account the Coulomb enhancement factor and free carrier absorption but not bandgap renormalization for the sake of simplicity. We assumed a parabolic conduction and two valence bands with the electron, light- and heavy-hole effective masses of 0.14 m_0 [22], 0.082 m_0 and 0.5 m_0, respectively, where m_0 is the electron rest mass.

The result of the calculation with the photocarrier density of 9.7×10^{16} cm^{-3} (laser intensity of 1 mW), $\tau_{\mathrm{cool}} = 5.3$ ps and $\tau_{\mathrm{decay}} = 400$ ps (figure 4(b)) is in good agreement with the OPPR traces, indicating that the shorter time constant τ_1^{OPPR} is attributed to the carrier cooling time τ_{cool}, while the longer one τ_2^{OPPR} contributes to the carrier decay time τ_{decay}.

Since it is difficult to accurately determine the spot diameter, and hence the effective laser intensity on the samples, the photocarrier densities may differ between OPPR and SPPX-STM measurements. This may cause a difficulty in the direct comparison of the lifetime with the SPPX-STM time constants if the lifetime is dependent on the laser intensity. This is not the case, as is revealed by the decay time dependence on the pump intensity (figure 4(c)). The values of τ_2^{OPPR} are almost constant for different intensities. We took the average of τ_2^{OPPR} obtained for the different intensities, 400±40 ps, as the value of the carrier lifetime. The lifetime obtained is almost the same as that, 360 ± 160 ps, similarly estimated from the OPPR traces with the excitation wavelength of 920 nm. The consistency of the lifetime analysis using different wavelengths confirms the validity of the estimation method, because photocarrier lifetimes in semiconductors should be only weakly dependent on the excitation wavelength [24].

These results indicate that the estimated photocarrier lifetime (=400 ± 40 ps) should be related to the slower decay component ($\tau_2^{\mathrm{STM}} = 550$ ps) of the ΔI curve that also reflects the carrier lifetime through the decay process of SPV.

5. Comparison of photocarrier lifetime determined by OPPR with SPPX-STM signal

The photocarrier lifetime τ_{decay} (=400 ± 40 ps) determined from the OPPR measurement is close to τ_2^{STM} (=550 ps) in the SPPX-STM signal, as expected. However, τ_2^{STM} is slightly longer than τ_{decay}. In order to clarify this point, we recall the fact that the exponential decay of a sample parameter does not appear in the ΔI curve as an exponential function. Furthermore, the apparent timescale of the calculated ΔI curve can be different from τ_{decay}. Therefore, the fitting procedure with exponential functions for ΔI curves yields an approximation for deriving decay times of the sample parameters. For saturation-prone nonlinearity, the apparent decay time in the calculated ΔI curve is longer than the carrier lifetime, as reported in the previous paper [12]. Experimentally, τ_2^{STM} is slightly longer than the estimated carrier lifetime τ_{decay}, which is in good agreement with the theoretical results.

6. Conclusion

We examined how the photocarrier dynamics is observed in the SPPX-STM signal (ΔI curve), using the results of OPPR measurements and of the analysis based on the nonlinear relationship between the photocarrier density and the tunnelling current. A comprehensive explanation was obtained for the SPPX-STM signal using the model based on the photocarrier dynamics that produces the surface photovoltage effect. This new technique is expected to contribute to the advance of future research in nanoscale science and technology, in terms of the ultimate temporal and spatial resolutions.

Acknowledgments

This work was supported in part by a Grant-in-Aid for Scientific Research from the Ministry of Education, Culture, Sports, Science, and Technology of Japan. We thank Professor Yoshitaka Okada and Dr Ryuji Oshima at the University of Tsukuba for their help with sample preparation and the photoluminescence study. We also thank Ms Rie Yamashita in our group at The University of Tsukuba for her help in preparing this paper.

References

[1] Weiss S, Botkin D, Ogletree D F, Salmeron M and Chemla D S 1995 *Phys. Status Solidi* b **188** 343
[2] Freeman M R, Elezzabi A Y, Steeves G M and Nunes G Jr 1997 *Surf. Sci.* **386** 290
[3] Khusnatdinov N N, Nagle T J and Nunes G Jr 2000 *Appl. Phys. Lett.* **77** 4434
[4] Hamers R J and Cahill D G 1991 *J. Vac. Sci. Technol.* B **9** 514
[5] Feldstein M J, Vohringer P, Wang W and Scherer N F 1996 *J. Phys. Chem.* **100** 4739
[6] Gerstner V, Knoll A, Pfeiffer W, Thon A and Gerber G 2000 *J. Appl. Phys.* **88** 4851
[7] Groeneveld R H M and van Kempen H 1996 *Appl. Phys. Lett.* **69** 2294
[8] Takeuchi O, Morita R, Yamashita M and Shigekawa H 2002 *Japan. J. Appl. Phys.* **41** 4994
[9] Yamashita M, Shigekawa H and Morita R 2005 *Mono-Cycle Photonics and Optical Scanning Tunneling Microscopy Route to Femtosecond Angstrom Technology* (*Springer Series in Optical Sciences* vol 99) (Berlin: Springer)
[10] Takeuchi O, Aoyama M, Oshima R, Okada Y, Oigawa H, Sano N, Shigekawa H, Morita R and Yamashita M 2004 *Appl. Phys. Lett.* **85** 3268
[11] Takeuchi O, Aoyama M and Shigekawa H 2005 *Japan. J. Appl. Phys.* **44** 5354
[12] Takeuchi O, Aoyama M, Kondo H, Taninaka A, Terada Y and Shigekawa H 2006 *Japan. J. Appl. Phys.* **45** 1926
[13] Shigekawa H, Takeuchi O and Aoyama M 2005 *Sci. Technol. Adv. Mater.* **6** 582
[14] Yoshida S, Kikuchi J, Kanitani Y, Takeuchi O and Shigekawa H 2005 *Surf. Sci. Technol.* **14** 192 (e-journal)
[15] Cahill D G and Hamers R J 1991 *J. Vac. Sci. Technol.* B **9** 564
[16] Aloni S, Nevo I and Haase G 2001 *J. Chem. Phys.* **115** 1875
[17] Takeuchi O, Yoshida S and Shigekawa H 2004 *Appl. Phys. Lett.* **84** 3645
[18] Othonos A 1998 *J. Appl. Phys.* **83** 1789
[19] Perkins J D, Mascarenhas A, Zhang Y, Geisz J F, Friedman D J, Olson J M and Kurtz S R 1999 *Phys. Rev. Lett.* **82** 3312
[20] Klar P J, Grüning H, Heimbrodt W, Koch J, Höhnsdorf F, Stolz W, Vicente P M A and Camassel J 2000 *Appl. Phys. Lett.* **76** 3439
[21] Shan W, Walukiewicz W, Ager J W III, Haller E E, Geisz J F, Friedman D J, Olson J M and Kurtz S R 1999 *Phys. Rev. Lett.* **82** 1221
[22] Masia F *et al* 2006 *Phys. Rev.* B **63** 073201
[23] Prabhu S S and Vengurlekar A S 2004 *J. Appl. Phys.* **95** 7803
[24] Yu J-S, Horng S-Fu and Chi C-C 1998 *Japan. J. Appl. Phys.* **37** 554